


Critical point for demixing of binary hard spheresHideki Kobayashi ¹, Paul B. Rohrbach ², Robert Scheichl ^{3,4}, Nigel B. Wilding ⁵, and Robert L. Jack ^{1,2}¹*Yusuf Hamied Department of Chemistry, University of Cambridge, Lensfield Road, Cambridge CB2 1EW, United Kingdom*²*DAMTP, University of Cambridge, Centre for Mathematical Sciences, Wilberforce Road, Cambridge CB3 0WA, United Kingdom*³*Institute for Applied Mathematics, Heidelberg University, INF 205, 69120 Heidelberg, Germany*⁴*Department of Mathematical Sciences, University of Bath, Bath BA2 7AY, United Kingdom*⁵*H. H. Wills Physics Laboratory, University of Bristol, Royal Fort, Bristol BS8 1TL, United Kingdom* (Received 8 April 2021; revised 1 July 2021; accepted 22 September 2021; published 8 October 2021)

We use a two-level simulation method to analyze the critical point associated with demixing of binary hard-sphere mixtures. The method exploits an accurate coarse-grained model with two- and three-body effective interactions. Using this model within the two-level methodology allows computation of properties of the full (fine-grained) mixture. The critical point is located by computing the probability distribution for the number of large particles in the grand canonical ensemble and matching to the universal form for the 3D Ising universality class. The results have a strong and unexpected dependence on the size ratio between large and small particles, which is related to three-body effective interactions and the geometry of the underlying hard-sphere packings.

DOI: [10.1103/PhysRevE.104.044603](https://doi.org/10.1103/PhysRevE.104.044603)**I. INTRODUCTION**

Hard-sphere systems are central to our understanding of many physical systems and phenomena, including the structure of the liquid state [1]; the behavior of colloidal suspensions [2–4]; jamming and glass transitions [5,6]; and packing problems [7,8]. In equilibrium statistical mechanics, hard-particle systems are simple and elegant, because every allowed configuration has the same statistical weight. Despite this simplicity, these systems are of practical importance: they are amenable to experiments [2,4,5,9]; and they support complex behavior including a variety of phase transitions [10–15], which continue to challenge theoretical and computer simulation methods. We focus here on *mixtures of large and small hard spheres*, which are predicted to undergo fluid-fluid phase separation (demixing), if the size disparity and the concentrations are large enough [16–21]. The phase where the large particles predominate corresponds to a (metastable) colloidal liquid [22]. Contrary to the usual intuition that liquids are stabilized by attractive forces, this phase appears in an equilibrium system with additive mixing rules and without any attractive forces between particles. This illustrates the depletion mechanism for demixing [22–24], which is one of the prototypical mechanisms for fluid-fluid phase separation.

Given its status as a theoretical benchmark, it may be surprising that this fluid-fluid phase separation of hard spheres has never been accurately characterized. Buhot and Krauth [25] showed that large particles cluster together strongly, in small systems at moderate overall volume fractions; Dijkstra, van Roij, and Evans [26] analyzed fluid-solid and solid-solid demixing. These numerical studies confirm that depletion leads to strong effective interactions in these systems [25], whose behavior is captured semiquantitatively by theoretical

arguments [16,19,20]. However, the critical point for demixing has never been observed directly, nor have the coexisting fluid phases.

The reason for this state of affairs is that demixing involves collective behavior of the large particles, which can be observed only if their number is great enough. Additionally, a depletion effect that is strong enough to produce demixing requires a large disparity in size between the particles, and a large concentration of the small particles. Hence one must analyze configurations with very many small particles, and there is also a huge disparity between the timescales on which the two species relax. Figure 1 illustrates the severe challenges that this poses for computer simulation: the systems are extremely crowded, and they include many particles of disparate sizes, with significant interparticle correlations. This complexity also means that exact theoretical computations are out of reach, so efficient numerical methods are necessary for accurate results.

This work uses a two-level numerical method [27] to characterize the critical point for fluid-fluid phase separation in hard-sphere mixtures. The first level of the method relies on an accurate coarse-grained (CG) model where the small particles are integrated out, providing an effective theory for the large ones. Then, the second level restores the small particles, providing (numerically) exact results for the full mixture. The method was previously validated for the Asakura-Oosawa model [23], which is a much simpler example of demixing, for which an exact CG model is available. The results presented here show that the method is viable in complex systems, finally allowing direct observation of the phase transition in the hard-sphere system. The results also reveal new physics, in that the packing of the hard particles influences the phase transition via three-body depletion interactions, which have been neglected in previous theories [16,19–21,28,29]. As such, our

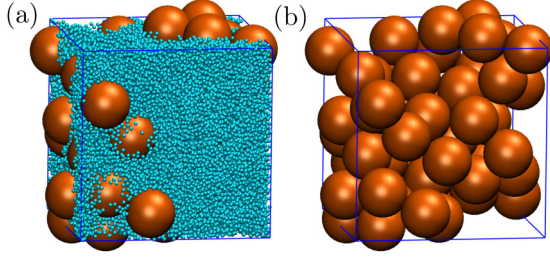


FIG. 1. (a) Snapshot of a binary hard-sphere system at size ratio 11:1, near criticality ($\eta_S^r = 0.302$). The box size is $\tilde{L} = 44$, and there are $N = 50$ large particles. (b) The same configuration with the small particles removed; this is a configuration of the CG model.

results confirm the qualitative picture proposed in [16,19,20], so that arguments against fluid-fluid demixing are not correct [30,31]. But they also highlight that the standard two-body depletion theories are not adequate for accurate characterization of this important phase transition [32,33] (see also [27,34] for a discussion of their effects in the Asakura-Oosawa model).

The paper is organized as follows: Sec. II introduces the model and the relevant theory. Then Sec. III presents results for the critical point of the hard-sphere mixture, and Sec. IV assesses the accuracy and efficiency of the method. A summary and outlook is given in Sec. V. We also include Appendixes with additional theoretical details (Appendix A), computational details (Appendix B), and information about the CG model that we have developed (Appendix C).

II. HARD SPHERE MODEL AND ITS CRITICAL POINT

A. Fine-grained model

We analyze a binary mixture of hard spheres whose diameters are σ_S (small particles) and $\sigma_B = \ell\sigma_S$ (big particles, so $\ell > 1$). We use a cubic simulation box of linear size L with periodic boundaries, in the grand canonical ensemble. A configuration of the system has N large particles with positions $\mathbf{R}_1, \dots, \mathbf{R}_N$ and n small particles with positions $\mathbf{r}_1, \dots, \mathbf{r}_n$. The relevant dimensionless parameters are the size ratio ℓ , the system size $\tilde{L} = L/\sigma_S$ and the chemical potentials μ_B, μ_S (measured relative to $k_B T$). Further details of the model and the underlying theory are given in Appendix A. We parameterize μ_S in terms of the (reservoir) small-particle volume fraction η_S^r , using an accurate equation of state [35].

Figure 2(c) illustrates the phase diagram proposed in [19,20]. As a signature of demixing, we seek the critical point. Define $p(N)$ as the probability that the system contains N large particles. For large systems in a single-phase regime, $p(N)$ is unimodal and Gaussian. As one approaches the critical point (μ_B^*, η_S^{r*}), the distribution $p(N)$ broadens; at the critical point the large particles form a fractal structure, and $p(N)$ has a characteristic (universal) scaling form [36,37]. For $\eta_S^r > \eta_S^{r*}$ one expects a phase coexistence line in the (μ_B, η_S^r) plane, where $p(N)$ is bimodal.

We locate the critical point by matching the observed $p(N)$ to its universal scaling form [37,38], corresponding to the 3D Ising universality class. Since N (or equivalently the concentration N/\tilde{L}^3) is the natural order parameter for the demixing

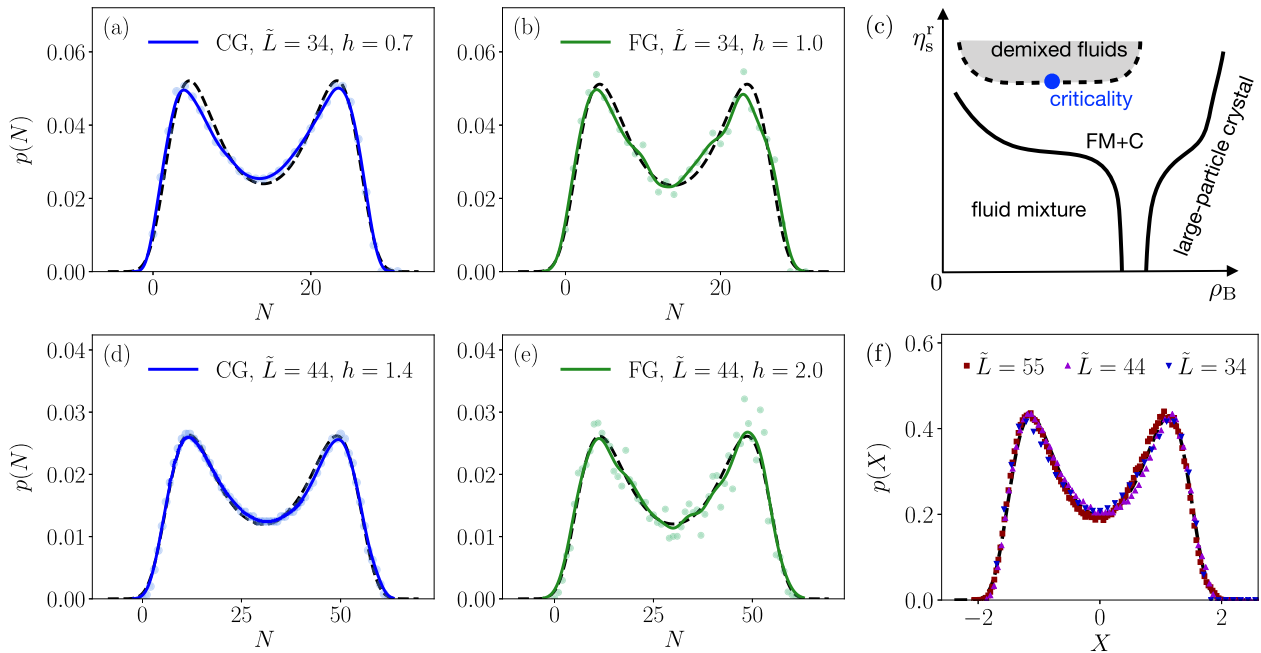


FIG. 2. Results for $\ell = 11$. Histograms for the number of large particles for CG model (a, d) and FG model (b, e), with $\eta_S^r = 0.3020, 0.3010$ for $\tilde{L} = 34, 44$, respectively. The universal critical form [36] is shown by dashed lines. The underlying data are shown as points and the solid lines are Gaussian kernel density estimates with width parameters h as shown. (c) Schematic phase diagram, following [20], as a function of $\rho_B = N/\tilde{L}^3$ and η_S^r . The critical point for demixing is indicated, together with the coexistence region (shaded). The demixed state is metastable with respect to crystallization of the large particles (the coexistence region between a fluid mixture and a crystal is labeled as FM + C). The region of coexistence between two crystal phases is omitted for simplicity; see [20]. (f) Finite-size scaling collapse for coarse-grained data at $\tilde{L} = 34, 44, 55$; results for $\tilde{L} = 55$ have $\eta_S^r = 0.3006$.

transition, it is natural to work in the grand canonical ensemble, where the finite-size scaling of the critical fluctuations is well understood [37].

Sampling $p(N)$ is not tractable by standard methods—it requires that large particles are inserted and removed from the system, which is almost impossible in crowded environments like that shown in Fig. 1. This problem is avoided by the two-level method. We outline the approach; see [27] and Appendix A for details. The critical points of interest generically occur for parameters where the fluid phase is metastable with respect to crystallization of the large particles [20] [recall Fig. 2(c)]; in fact, the two-level method helps to control for crystallization (see Sec. IV B below).

B. Coarse-grained model

The method relies on a coarse-grained (CG) model, where the small particles are integrated out, leaving only the large ones. It involves an effective interaction among the large particles, the corresponding energy is

$$E_{CG}(C) = N\Delta\mu + \sum_{1 \leq i < j \leq N} V_2(R_{ij}) + \sum_{1 \leq i < j < k \leq N} V_3(R_{ij}, R_{ik}, R_{jk}), \quad (1)$$

where $R_{ij} = |\mathbf{R}_i - \mathbf{R}_j|$ is the distance between particles i and j ; also V_2 and V_3 are two- and three-body effective interactions, and the term $N\Delta\mu$ ensures that the chemical potentials coincide between FG and CG models. The $\Delta\mu$, V_2 , V_3 are obtained by grand-canonical Monte Carlo (GCMC) simulation of small particles in systems which contain a few fixed large particles; see [27] and Appendix B.

The resulting CG model is highly accurate but it is not a perfect description of the large-particle behavior. Hence the second step of the method, which computes the difference between the coarse-grained result and the result for the full [fine-grained (FG)] model. Recalling that $p(N)$ is the probability that the FG model has N large particles, define $p_{CG}(N)$ as the corresponding quantity for the CG model. Then

$$p(N) = p_{CG}(N) + \Delta p(N), \quad (2)$$

where $\Delta p(N)$ is the coarse-graining error.

The distribution p_{CG} is computed by GCMC simulation of the CG model and the correction Δp is calculated following [27], using a free-energy estimate based on Jarzynski's equality [39–42]. The computation of $\Delta p(N)$ distinguishes our approach from traditional coarse-graining methods [43–47] in which the main concern is that the CG model is as accurate as possible, but its error is not usually quantified. In practice, our CG model is accurate enough that the correction Δp will turn out to be small. (Computation of this correction has similarities with free-energy perturbation theory [48], as recently exploited to correct coarse-graining errors for machine-learned potentials [49]).

III. RESULTS: CRITICAL POINT

A. Size ratio 11:1 ($\ell = 11$)

We begin with results that demonstrate the critical point in a mixture with $\ell = 11$. The CG model was computed

following Appendix B, details of the interactions are given in Appendix C.

Figure 2 shows results at the critical point. For a tractable analysis, we considered relatively small system sizes $\tilde{L} = 34, 44$, which are between three and four times the diameter of a large particle. The behavior of $p_{CG}(N)$ is shown in Figs. 2(a) and 2(d). By adjusting η_S^c and μ_B , we obtained estimates of the critical point, where the distribution p_{CG} matches its universal critical form (black dashed line), which has been scaled to give the correct mean and variance. The systems are small but the fit to the universal form is good. The agreement with the universal distribution ensures that cumulant ratios [50] are also in agreement with their universal values at criticality.

Turning to the FG model, we estimate the correction Δp , and hence the distribution $p(N)$ for the binary mixture. The method requires M configurations of the CG model which we denote as C_1, C_2, \dots, C_M , obtained by GCMC simulation. (Specifically, we take $M = 1280$). For each coarse configuration, we then perform a GCMC simulation for the small particles, with the large ones held fixed. This yields a reweighting factor $\hat{\omega}_\alpha$ (see Appendix A), then $\Delta p(N)$ is estimated as

$$\Delta \hat{p}(N) = \sum_{\alpha=1}^M (\hat{\omega}_\alpha - 1) I_N(C_\alpha), \quad (3)$$

where $I_N(C_\alpha) = 1$ if C_α contains N large particles, and $I_N(C_\alpha) = 0$ otherwise.

Results for $p(N)$ are shown in Figs. 2(b) and 2(e), including individual estimates of $p(N)$, and (smoothed) kernel density estimates of p , based on the same data. The resulting distributions match the universal scaling form, indicating that the FG model is indeed very close to its critical point; see also [37,51]. The large-particle volume fraction at criticality is estimated at $\eta_B^* \approx 0.25$, which is broadly consistent with other estimates [20,28] and with general expectations for systems with very short-ranged attraction [52,53]. For a finite-size scaling analysis, we recenter and scale the particle number N to zero mean and unit variance:

$$X = \frac{N - \langle N \rangle}{\Delta_N}, \quad \Delta_N = \sqrt{\langle N^2 \rangle - \langle N \rangle^2}. \quad (4)$$

Figure 2(f) shows additional finite-size scaling results for the CG model at $\ell = 11$, including results at a larger system size $\tilde{L} = 55$. These results are consistent with behavior in the Ising universality class, although the systems are small enough that corrections to scaling are significant; see [37] and Sec. III D.

It can be shown that the estimates of $p(N)$ are asymptotically unbiased [27], but they do suffer from large variance if either (1) the CG model is not sufficiently accurate or (2) the free-energy computations are performed too quickly [54]. These effects can lead to fat-tailed distributions of reweighting factors $\hat{\omega}_\alpha$, so that the estimate $\Delta \hat{p}$ starts to be dominated by a few (nontypical) configurations C_α . This can be easily checked from the numerical data, providing a consistency check on the method. In fact efficient performance with moderate M (as used here) requires a typical coarse-graining error significantly less than $k_B T$ in the total energy E_{CG} .

The behavior of the weights $\hat{\omega}_\alpha$ is discussed in Sec. IV, showing that this condition holds. We also note the FG data

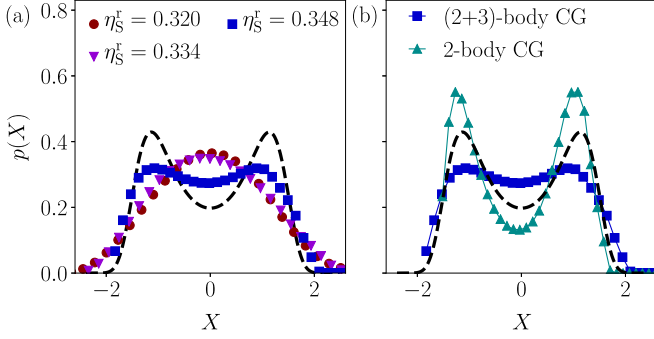


FIG. 3. Distributions of the order parameter X in the CG model at $\ell = 10$. The system size is $L = 3\sigma_B$ (so $\tilde{L} = 30$), dashed lines indicate the universal critical form. (a) Results for increasing η_S^t , indicating that $\eta_S^* \gtrsim 0.348$ (the results at this largest η_S^t appear close to criticality, but demixing has not yet occurred). (b) Comparison of the CG model (1) [labeled as (2+3)-body] and a two-body CG model ($V_3 = 0$), both at $\eta_S^t = 0.348$. The three-body interaction suppresses demixing.

points in Fig. 2 are scattered around the kernel density estimate, this indicates the size of the numerical errors (which would be very large if the CG model was not accurate).

B. Size ratio 10:1 ($\ell = 10$)

In contrast to the results for $\ell = 11$, the behavior of the CG system for $\ell = 10$ is shown in Fig. 3(a), for a small system $L = 3\sigma_B$. The distributions of X in Fig. 3(a) are “less bimodal” than the (universal) critical form, indicating that if this system has a critical point, it has $\eta_S^* \gtrsim 0.35$. For such high-volume fractions, any computations involving small particles become challenging, including accurate estimation of the coarse-graining potential, so we have not explored further into this regime. In the range shown, the three-body effective interactions for $\ell = 10$ are repulsive, especially for larger η_S^t ; see Appendix C. To illustrate their effect, Fig. 3(b) compares the CG model with a similar (2-body CG) model without any three-body interactions ($V_3 = 0$). For the two-body CG model, it is clear that $\eta_S^* < 0.348$, but the three-body interaction drives the critical point to larger η_S^t .

To summarize: Fig. 2 demonstrates a demixing critical point in CG and FG models of binary hard spheres with $\ell = 11$ and $\eta_S^* \approx 0.30$, but Fig. 3 shows that for $\ell = 10$ the corresponding critical point is beyond the reach of our numerics, $\eta_S^* \gtrsim 0.35$. For $\ell = 10$, previous estimates of η_S^* [16,19–21,28] were smaller (0.29–0.32), but such treatments assumed that two-body CG models are accurate. Figure 3(b) shows explicitly that three-body effective interactions suppress demixing at $\ell = 10$, explaining the difference in η_S^* . By contrast, for $\ell = 11$ the two-body CG model is more accurate; indeed, the Noro-Frenkel criterion [52] holds quite accurately at the critical point (see Sec. III D below).

C. Differences between $\ell = 10, 11$

For a physical explanation of these substantial differences between $\ell = 10, 11$, note that demixing is favored if the colloidal liquid (large- N) phase supports efficient packing. The depletion effect makes it likely that large particles are very

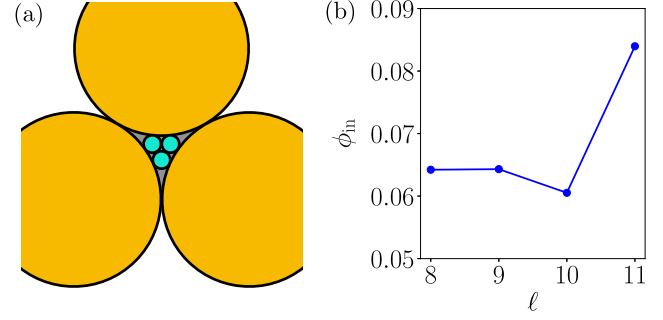


FIG. 4. Packing of large and small particles. (a) Planar configuration with three large particles touching each other and three small particles in the (gray shaded) space between them. (b) Measure of packing efficiency ϕ_{in} as defined in the discussion, for $\eta_S^t = 0.32$. This quantity increases sharply between $\ell = 10$ and $\ell = 11$.

close to each other, so it matters whether the small particles pack efficiently into the gaps between them.

To understand a key difference between hard-sphere packing at $\ell = 10, 11$, note that planar configurations similar to Fig. 4(a) are efficient for packing, but they are possible only for $\ell \geq 5 + \sqrt{24} \approx 9.9$. Hence, such configurations are very rare for $\ell = 10$ (which is close to the marginal case), but they are much more common for $\ell = 11$.

To show this explicitly, we used GCMC simulation for small particles to compute a (normalized) number density ϕ_{in} in the shaded gray region of Fig. 4(a), which we interpret as a measure of packing efficiency. Specifically, we fix three large particles in mutual contact [as in Fig. 4(a)] and simulate the small particles in the grand canonical ensemble. Let n_Δ be average number of small particles within the shaded gray area of Fig. 4(a) (more precisely, we take a three-dimensional region that extends above and below the plane of the figure by a distance $\delta z/2$ in each direction). The area of the shaded region is $A_\Delta = (2\sqrt{3} - \pi)\sigma_B^2/8$ and

$$\phi_{in} = \frac{\sigma_S^3}{\delta z A_\Delta} n_\Delta \quad (5)$$

is the number density in the relevant volume (in units of σ_S^{-3}). This quantity depends on the small-particle volume fraction, the comparison in Fig. 4 is at $\eta_S^t = 0.32$, and we take $\delta z = \sigma_S$. For very large ℓ then ϕ_{in} tends to the bulk number density but its behavior for moderate ℓ is subtle, because of the complexity of the underlying sphere packings. For the representative volume fraction $\eta_S^t = 0.32$, Fig. 4(b) shows that the packing efficiency ϕ_{in} increases sharply between $\ell = 10$ and $\ell = 11$, which we interpret as a contributing factor to the enhanced demixing at $\ell = 11$.

Other signatures of more efficient packing at $\ell = 11$ are discussed in Appendix C. We note from those results that while the packing around triplets of large particles enters the three-body effective interaction, there are also nontrivial packing effects for small particles that are close to two large ones. This can be seen from the nontrivial form of the two-body interaction. Such interactions are partially captured by the predictions of density functional theory (DFT) [21], but as η_S^t increases, there are increasing differences between the

predictions of DFT and the numerically computed potential—these are also due to packing effects, which are not captured accurately by simple density functionals [33].

D. Critical behavior—Discussion

This section discusses some physical features of the critical point for demixing that we have found and some further details of the results.

1. Finite-size effects and field mixing in $p(N)$

The systems considered in this work are relatively small, compared to the diameter of the large particles, which does affect the results. However, the finite-size scaling theory of the critical point is well developed [37], which allows these effects to be rationalized. In particular, one sees from Figs. 2(a) and 2(d) that the probability $p(0)$ is not completely negligible, so the system may contain no large particles at all. The universal form is relevant for large N —it does not account for the fact that this number is an integer, nor that it must be non-negative. Hence one cannot expect an exact match to this form in small systems. So-called field-mixing effects arising from the lack of symmetry between the fluid phases [37] can also lead to asymmetry in $p(N)$, resulting in deviations from the (symmetric) scaling form for finite-sized systems. Larger systems would allow a more detailed analysis of these effects, as well as estimation of critical exponents. However, given the various types of corrections to scaling that should be expected, the close agreement observed here between the numerical data and the universal form is remarkable, and represents strong evidence for a demixing critical point.

2. Extended law of corresponding states

Noro and Frenkel [52] proposed that critical points for systems with short-ranged attractive (two-body) potentials can be estimated by a criterion based on the reduced second virial coefficient, which in this context is $B_2^* = (3/\sigma_B^3) \int_0^\infty [1 - e^{-V_2(r)}] r^2 dr$. (The factor of 3 is included so that $B_2^* = 1$ for a hard-sphere potential). They defined

$$\tau = \frac{1}{4(1 - B_2^*)} \quad (6)$$

so that small positive τ corresponds to strong attractive interactions. For short-ranged attractive systems, they found that critical points generically occur for $\tau \approx 0.1$. For adhesive hard-sphere (AHS) models (corresponding to very short-ranged attractive attractions), it was later estimated [53] that $\tau \approx 0.113$ at criticality. This can be interpreted as an (extended) law of corresponding states [52].

For the potentials studied here, we find for the critical parameters $\ell = 11$ and $\eta_S^t \approx 0.30$ that $\tau = 0.11$. The three-body effect is weak at this state point: if we revert to a two-body CG model with the same parameters, the system is close to criticality. For $\ell = 10$, Fig. 3(b) indicates that the two-body CG system is critical for η_S^t slightly below 0.348, corresponding again to $\tau \approx 0.1$, similar to [33]. These results are consistent with the extended law of corresponding states. Note, however, that the two-body CG system is not an accurate description of the full mixture at $\ell = 10$ because of the three-body effective

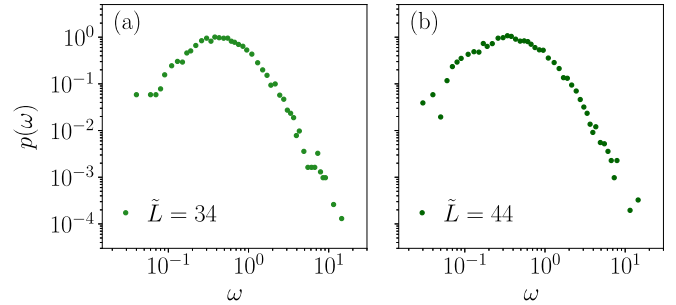


FIG. 5. Distributions of the reweighting factors ω_α for the FG models of Fig. 2. The important feature is that large reweighting factors (above $\omega = 10$, for example) are rare.

interactions (recall Fig. 3). Hence, the Noro-Frenkel criterion does not provide an accurate estimate of the critical behavior of the binary mixture, in that case.

3. Behavior for very large ℓ

We offer a few comments on the limit of large ℓ , corresponding to very extreme size ratio. This limit $\ell \rightarrow \infty$ is quite subtle [20]. It is convenient to fix σ_B and take $\sigma_S \rightarrow 0$. This can be done in three different ways: (1) keeping the concentration of small particles constant [55], (2) keeping the volume fraction of small particles constant [56], and (3) keeping the second virial coefficient B_2^* constant, for the effective interactions [57].

There is obviously no demixing in case (1) [55], and crystallization tends to dominate in case (2) [20]. As noted in [53], the relevant case for fluid-fluid demixing is (3). In this case one expects [20] that $\eta_S^t \sim (1/\ell) \log \ell$, which tends to zero $\ell \rightarrow \infty$. For very small η_S^t , interactions among the small particles can be neglected and we expect the system to behave similarly to an Asakura-Oosawa model, with a short-ranged two-body attraction, and negligible three-body and higher contributions. The qualitative behavior that we find for $\ell = 11$ is consistent with this physical picture: that two-body interactions dominate for very large ℓ and fluid-fluid demixing should occur. However, it is not clear how large ℓ should be in general, for three-body interactions to have a negligible effect.

IV. ACCURACY AND EFFICIENCY OF TWO-LEVEL METHOD

A. Reweighting factors and model accuracy

As a consistency check between the CG and FG models, Fig. 5 shows the distribution of the reweighting factors $\hat{\omega}_\alpha$ that appear in (3). This distribution has $\langle \hat{\omega} \rangle = 1$ by construction, but its variance has a significant impact on the results of the two-level method. In particular, if the CG model is not accurate (or the Jarzynski integration has large variance) then there will be some configurations with very large ω_α : these tend to dominate the estimate (3), resulting in a large statistical uncertainty in $\Delta \hat{p}$. (An example of this effect was shown in [27]).

Both histograms in Fig. 5 show a few samples with $\hat{\omega} \approx 10$, which have some impact on the FG results in Fig. 2. In particular, the data for $\tilde{L} = 44$ are somewhat scattered in that

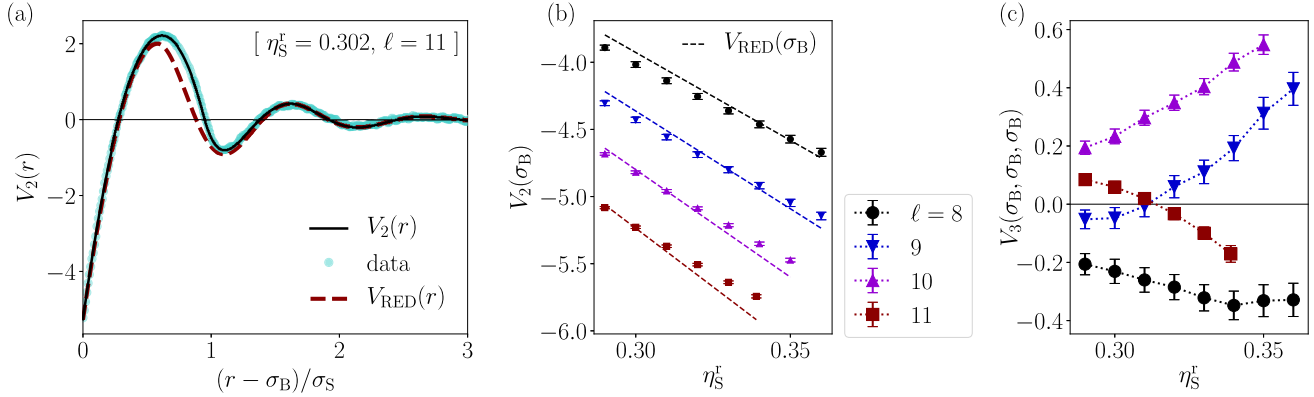


FIG. 6. CG model. (a) Tabulated two-body interaction $V_2(r)$ for parameters $\eta_S^c = 0.302$ and $\ell = 11$ (close to the critical point). This is shown together with the data from which it is estimated. The RED potential [21] is shown for comparison; it is mostly consistent with the data, but it underestimates the repulsive part of the potential. (b) The strength of the two-body interaction is illustrated using the value of the potential V_2 when the particles are touching. The strength increases (that is, the potential becomes more negative) on increasing η_S^c and ℓ . Dashed lines are a comparison with the RED potential. (c) The strength of the three-body interaction is illustrated using the value of V_3 when all three particles are touching. The dependence on the model parameters is more complicated in this case, as we discuss. Dotted lines are guides to the eye.

figure. Still, the kernel density estimate for $p(N)$ reduces the uncertainty by averaging over several values of N and appears to yield reliable estimates.

An ideal numerical computation would have $\hat{\omega}_\alpha = 1$ for all configurations—this is possible only if the CG model is perfectly accurate and the Jarzynski integration is carried out quasi-statically. As an indication of the differences between this (ideal) case and our practical computation, we show in Appendix C 3 that $\hat{D} = -\frac{1}{M} \sum_\alpha \log \hat{\omega}_\alpha$ is an estimated upper bound on the KL divergence (or relative entropy) between our CG model and a (putative) “perfect CG model” that captures the full (many-body) effective interaction potential. From the distributions of Fig. 5, we estimate $\hat{D} \approx 0.32$ for $\bar{L} = 34$ and $\hat{D} \approx 0.37$ for $\bar{L} = 44$. Hence, the error of the (total) energy of a configuration in the CG model is less than 0.4 (in units of $k_B T$, relative to an exact coarse-grained model). Since these are total energies for systems with significant numbers of particles, this indicates that the two- and three-body interactions are indeed accurate.

Note, however, that this high accuracy is essential for the two-level method to be effective. Since the (total) CG energy enters $\hat{\omega}_\alpha$ through an exponential, the numerical uncertainties in Δp grow quickly if typical errors on the CG energy start to be comparable with $k_B T$, or larger [27]. This is the main limitation in general application of such methods—very accurate CG models are required.

B. The role of crystallization

An additional advantage of the two-level method arises because the critical point in binary hard-sphere systems is metastable to crystallization. In our study, crystallization of the large particles was sometimes observed during simulation of the CG model. Crystallization must eventually occur in any accurate simulation of the large particles, because of the metastability. However, the critical point is sufficiently metastable that typical simulation runs can fully explore the critical distribution of N before crystallization takes place.

This effect is discussed in [28]; see, for example, Fig. 6 of that work. (Crystallization can be identified quite easily because N increases sharply to a large value that is typical for the crystal but is not representative of the fluid phases. Similar to [28], we found typical times before crystallization were of order 10^8 – 10^9 Monte Carlo sweeps). As a practical solution to this problem, we take the simple approach of discarding those CG simulation runs where crystallization occurs. Since the CG model is relatively easy to simulate, this still allows generation of sufficient data, at manageable cost. By contrast, methods that require full simulation of the FG model tend to be frustrated by crystallization, because they require large quantities of costly data to be discarded. Other solutions to this crystallization problem could also be considered, including different criteria for identifying crystalline states. However, since the system is able to explore the (metastable) critical distribution of N before crystallization, we expect that different approaches would lead to very similar results. The approach taken here amounts to a dynamical definition of the metastable state, as the state that is explored in simulations before crystallization occurs.

V. OUTLOOK

A. Demixing transitions

The main result of this work is that we have characterized the demixing critical point of hard-sphere mixtures at $\ell = 11$. This proved a challenging task, because of the scale separation between large and small particles (necessitating the use of a CG model), and the fact that the effective interactions among the large particles are complex, with strong dependence on ℓ .

We recall from the Introduction that these binary hard-sphere mixtures are prototypical model systems, which we use to gain generic insight into colloidal systems. We do not expect that the details of the three-body interactions derived here will be generic. For example, realistic colloidal systems have some polydispersity which would likely disrupt the idealized situation shown in Fig. 4(a), and spheres with perfectly

hard interactions may also be unrealistic in generic colloidal systems [4] (especially since many practical depletants are polymers, which are certainly not hard).

With this in mind, we draw two generic conclusions from this work, beyond the characterization of the demixing critical point. First, we note that two-body CG models are widely used in soft matter [58], and such models are generally expected to be accurate in hard-sphere mixtures with large ℓ [19,20]. Since three-body interactions turn out to be relevant even in this case, our results indicate that caution is advisable when applying two-body CG models in generic soft matter systems [33]. Second, our results show the power of the two-level approach (or more general multiscale approaches), which can be used to obtain fully quantitative and accurate results for underlying fine-grained systems, if the effective interactions can be computed accurately.

B. Two-level method

We close with a few comments on the two-level method [27]. To characterize the critical point to high accuracy, we use GCMC simulation and match $p(N)$ to its critical form. In this setting, the two-level method sidesteps the problem of inserting large particles into the crowded environment shown in Fig. 1, because particle insertion is performed at the coarse-grained level, while the small particles appear only in the second (FG) level. The method requires a very accurate CG model [27] and considerable computational effort, but this is mitigated by the fact that the FG level is trivial to parallelize. This method falls into the general class of multilevel approaches [59–64]; the results presented here are further evidence that multilevel coarse-graining methods have useful application in the physical sciences [27,65–67] (see also [68–70]), especially if it can be combined with machine-learned effective potentials [71–74], similar to [49].

In principle, the methodology is very flexible, as long as suitable CG models can be derived (or inferred). For example, extensions to this work might include the solid-solid critical point that is predicted in hard-sphere mixtures [20], or hard-sphere mixtures in inhomogeneous settings, as commonly considered in density functional theory (see, for example, [75]). On the other hand, these methods are not trivial to apply—two requirements are a very accurate CG model, and a tractable method for computing the reweighting factors $\hat{\omega}_\alpha$ to sufficient accuracy. For the first, the limitation of our results to $\eta_S^t \leq 0.35$ (for $\ell = 10$) is partly because computation of a sufficiently accurate CG model becomes very challenging. (GCMC simulations of small particles at larger η_S^t become increasingly difficult). The same issue also hinders accurate computations of $\hat{\omega}_\alpha$. In addition, our limitation to relatively small systems arises because the computational time to obtain highly accurate reweighting factors $\hat{\omega}_\alpha$ grows with \bar{L} : the reweighting factors are obtained from small-particle free energies which must be computed to an *absolute* accuracy of order $k_B T$, while the absolute value of the free energy is growing proportional to the system volume \bar{L}^3 . This necessitates small relative errors, and makes simulations increasingly costly at large ℓ (because $\bar{L} \sim \ell$ if one increases the size ratio at fixed $\langle N \rangle$). These caveats should be borne in mind when applying the method to other systems. Nevertheless, we look forward

to future work exploiting these methods in soft matter systems and elsewhere.

ACKNOWLEDGMENTS

We thank Daan Frenkel and Bob Evans for helpful discussions. This project was supported by the Leverhulme Trust (Grant No. RPG-2017-203). R.L.J. and H.K. are also grateful to the EPSRC for support in the later part of the project (Grant No. EP/T031247/1).

APPENDIX A: THEORY

This Appendix describes the theory of the two-level method as it applies to binary hard-sphere mixtures.

1. FG model (binary mixture)

We define the relevant properties of the binary hard-sphere system (BHS) and the corresponding CG model. Following [27], we denote the large-particle (coarse) degrees of freedom by

$$\mathcal{C} = (N, \mathbf{R}_1, \dots, \mathbf{R}_N), \quad (\text{A1})$$

and the small-particle (fine) degrees of freedom by

$$\mathcal{F} = (n, \mathbf{r}_1, \dots, \mathbf{r}_n). \quad (\text{A2})$$

Define a function $e_{\text{BHS}}(\mathcal{C}, \mathcal{F})$ such that $e_{\text{BHS}} = 1$ if none of the hard spheres overlap each other, and $e_{\text{BHS}} = 0$ otherwise. Then the Boltzmann weight for any configuration of the BHS system is

$$w_{\text{BHS}}(\mathcal{C}, \mathcal{F}) = e_{\text{BHS}}(\mathcal{C}, \mathcal{F}) \frac{\exp(\mu_B N + \mu_S n)}{N! n!}, \quad (\text{A3})$$

and the probability density for configurations in the grand canonical ensemble is

$$p_{\text{BHS}}(\mathcal{C}, \mathcal{F}) = \frac{w_{\text{BHS}}(\mathcal{C}, \mathcal{F})}{\sigma_B^{3N} \sigma_S^{3n} \Xi}, \quad (\text{A4})$$

where the normalization constant Ξ is the grand-canonical partition function. Specifically

$$\Xi = \sum_{N,n} \int d\mathbf{R}_1 \dots d\mathbf{R}_N d\mathbf{r}_1 \dots d\mathbf{r}_n \frac{w_{\text{BHS}}(\mathcal{C}, \mathcal{F})}{\sigma_B^{3N} \sigma_S^{3n}}, \quad (\text{A5})$$

where each particle position is integrated over the simulation box (which is a cube of size L). Hence Ξ depends on $\ell, \mu_B, \mu_S, \bar{L}$.

Averages in the FG and CG models are denoted by $\langle \cdot \rangle_{\text{FG/CG}}$. Specifically, if A is an observable quantity in the FG model then

$$\langle A(\mathcal{C}, \mathcal{F}) \rangle_{\text{FG}} = \sum_{N,n} \int d\mathbf{R}^N d\mathbf{r}^n A(\mathcal{C}, \mathcal{F}) p_{\text{BHS}}(\mathcal{C}, \mathcal{F}), \quad (\text{A6})$$

where the integrals are over all particle positions, within the simulation box.

Here and in the following, note that weight functions like w_{BHS} are dimensionless (and not normalized as probability distributions), but p indicates a normalized probability density.

It is natural to define the small-particle volume fraction as

$$\eta_S = \frac{\pi}{6\tilde{L}^3} \langle n \rangle_{\text{FG}}. \quad (\text{A7})$$

The reservoir volume fraction η_S^r is the value of η_S that one obtains in a system with no large particles at all, as $\tilde{L} \rightarrow \infty$. This depends only on μ_S and can be estimated very accurately using the equation of state of [35]. This η_S^r depends monotonically on μ_S ; it is used to parameterize the dependence of the results on μ_S (whose value is not particularly intuitive) in terms of the more natural parameter η_S^r .

2. CG model

The coarse degrees of freedom \mathcal{C} from (A1) describe configurations of the CG model. Define $e_{\text{HS}}(\mathcal{C}) = 1$ if none of the large particles overlap with each other and $e_{\text{HS}}(\mathcal{C}) = 0$ otherwise, analogous to e_{BHS} above. The Boltzmann weight for the CG model is

$$w_{\text{CG}}(\mathcal{C}) = e_{\text{HS}}(\mathcal{C}) \frac{\exp[\mu_B N - E_{\text{CG}}(\mathcal{C})]}{N!}, \quad (\text{A8})$$

where the effective interaction energy E_{CG} is given in Eq. (1). Similar to the FG case define

$$p_{\text{CG}}(\mathcal{C}) = \frac{w_{\text{CG}}(\mathcal{C})}{\sigma_B^{3N} \Xi_{\text{CG}}}, \quad \Xi_{\text{CG}} = \sum_N \int d\mathbf{R}_1 \dots d\mathbf{R}_N \frac{w_{\text{CG}}(\mathcal{C})}{\sigma_B^{3N}}. \quad (\text{A9})$$

If A is an observable quantity in the CG model, then its average is

$$\langle A(\mathcal{C}) \rangle_{\text{CG}} = \sum_N \int d\mathbf{R}_1 \dots d\mathbf{R}_N A(\mathcal{C}) p_{\text{CG}}(\mathcal{C}). \quad (\text{A10})$$

3. Transformation between models and computation of Δp

To connect the CG and FG models, we (formally) integrate out the small particles from the FG model. The result is an effective Boltzmann weight for the large particles alone, which is

$$w_{\text{eff}}(\mathcal{C}) = \sum_{n=0}^{\infty} \int d\mathbf{r}_1 \dots d\mathbf{r}_n \frac{w_{\text{BHS}}(\mathcal{C}, \mathcal{F})}{\sigma_S^{3n}}. \quad (\text{A11})$$

Now define $\Phi(\mathcal{C})$ as the grand-canonical free energy of the small particles, evaluated for a fixed large-particle configuration \mathcal{C} :

$$\Phi(\mathcal{C}) = -\log \sum_{n=0}^{\infty} \int d\mathbf{r}_1 \dots d\mathbf{r}_n \frac{e_{\text{BHS}}(\mathcal{C}, \mathcal{F}) \exp(\mu_S n)}{\sigma_S^{3n} n!}. \quad (\text{A12})$$

[This quantity is finite as long as the large particles do not overlap, $e_{\text{HS}}(\mathcal{C}) = 1$. If $e_{\text{HS}}(\mathcal{C}) = 0$ then $e_{\text{BHS}}(\mathcal{C}, \mathcal{F}) = 0$ also, so $w_{\text{eff}}(\mathcal{C}) = 0$]. Comparing the integrals in the two preceding equations and using (A3), we find

$$w_{\text{eff}}(\mathcal{C}) = e_{\text{HS}}(\mathcal{C}) \frac{\exp[\mu_B N - \Phi(\mathcal{C})]}{N!}. \quad (\text{A13})$$

A perfect CG model would have $w_{\text{CG}}(\mathcal{C}) = w_{\text{eff}}(\mathcal{C}) / \Xi_0$ for some constant Ξ_0 (independent of \mathcal{C}): in this case the CG model would exactly reproduce the behavior of the large particles in the FG model. Comparing (A8) with (A13), this

amounts to $E_{\text{CG}}(\mathcal{C}) = \Phi(\mathcal{C}) + \log \Xi_0$. However, in the absence of an exact coarse-grained computation, such a perfect CG model is not available.

Still, one can make progress if the CG model provides a good approximation to w_{eff} , because averages in the FG and CG models are related. Let A be an observable quantity that depends only on the large particles. Combining the ingredients gathered above one finds

$$\langle A(\mathcal{C}) \rangle_{\text{FG}} = \frac{1}{Z} \left\langle A(\mathcal{C}) \frac{w_{\text{eff}}(\mathcal{C})}{w_{\text{CG}}(\mathcal{C})} \right\rangle_{\text{CG}}, \quad Z = \left\langle \frac{w_{\text{eff}}(\mathcal{C})}{w_{\text{CG}}(\mathcal{C})} \right\rangle_{\text{CG}}. \quad (\text{A14})$$

Now define $I_N(\mathcal{C})$ to be equal to unity if the system contains N large particles and zero otherwise. Hence $p(N) = \langle I_N(\mathcal{C}) \rangle_{\text{FG}}$, so using Eq. (3) with Eqs. (A8), (A13), and (A14) yields

$$\Delta p(N) = \left\langle I_N(\mathcal{C}) \left[\frac{W(\mathcal{C})}{Z} - 1 \right] \right\rangle_{\text{CG}} \quad (\text{A15})$$

with

$$W(\mathcal{C}) = \exp[E_{\text{CG}}(\mathcal{C}) - \Phi(\mathcal{C})]. \quad (\text{A16})$$

[Similarly, one may write $Z = \langle W(\mathcal{C}) \rangle_{\text{CG}}$. This means that if Φ can be computed (or estimated) then so can Δp , and hence also p . Moreover, (A15) is an average in the CG model, which is computationally tractable. The same idea is used in free-energy perturbation theory [48], to relate complicated models to simpler (more tractable) ones.

4. Estimation of small-particle free energy Φ

To make use of (3) in practice, we require a computational estimate of $W(\mathcal{C})$. The object $\Delta \hat{p}$ in (3) is an estimator for (A15), with \hat{w}_α in (3) corresponding to the ratio $W(\mathcal{C})/Z$ in (A15). We estimate $e^{-\Phi(\mathcal{C})}$ using a method based on Jarzynski's equality [39], as described in [27]. We give a short outline here. It is important that $\Phi(\mathcal{C})$ depends on the small-particle chemical potential μ_S via w_{BHS} . First select a very small chemical potential $\mu_S = \mu_0$, in which case the integral can be estimated directly from a grand canonical simulation. Denote the corresponding value of $\Phi(\mathcal{C})$ by $\Phi_0(\mathcal{C})$. Then, starting from an equilibrated system at chemical potential μ_0 , perform an GCMC simulation during which the small-particle chemical potential increases in K steps from μ_0 to μ_S . Then compute

$$\mathcal{I}(\mathcal{C}) = \sum_{j=1}^K n_j \Delta \mu_j, \quad (\text{A17})$$

where $\Delta \mu_j$ is the change in μ on the j th step and n_j is the number of small particles in the system when that step takes place. Since this quantity is the work done to insert the small particles, it follows from Crooks' theorem [40] that $e^{\mathcal{I}(\mathcal{C}) - \Phi_0(\mathcal{C})}$ is an unbiased estimate of $e^{-\Phi(\mathcal{C})}$. That is,

$$\langle e^{\mathcal{I}(\mathcal{C}) - \Phi_0(\mathcal{C})} \rangle_{\text{MC}} = e^{-\Phi(\mathcal{C})}, \quad (\text{A18})$$

where the average is over many realizations of the random MC algorithm (always with the same large-particle configuration \mathcal{C}). Hence

$$\hat{W}(\mathcal{C}) = e^{E_{\text{CG}}(\mathcal{C}) + \mathcal{I}(\mathcal{C}) - \Phi_0(\mathcal{C})} \quad (\text{A19})$$

is an unbiased estimate of $W(\mathcal{C})$. Note that this result does not depend on the parameters of the GCMC simulation that was used to compute \mathcal{I} . However, the variance of the estimate \hat{W} does depend strongly on these parameters, which must be chosen judiciously for the method to be effective.

In practice, each step in (A17) corresponds to one Monte Carlo sweep (corresponding to \tilde{L}^3 insertion and deletion attempts). The $\Delta\mu_j$ are adjusted so that one expects a typical change of δn_j in the average number of small particles on step j , for a bulk system of small particles alone. The value of δn_j depends on the overall volume fraction and on the accuracy required: Smaller values of δn lead to more accurate results (slower annealing during the integration of \mathcal{I}), but the computational expense is higher. Very small δn is required at large η_S^r , because of significant MC rejection rates in these crowded systems. Further details are given in the relevant sections below.

APPENDIX B: COMPUTATIONAL DETAILS

This Appendix explains the numerical procedures that are used to compute the CG interaction potentials in (1) and the reweighting factors $\hat{\omega}_\alpha$ that appear in (3).

1. Computation of CG potentials

For the two-body CG potential V_2 , consider a configuration \mathcal{C}_r that contains exactly two particles ($N = 2$), separated by a distance r . The exact two-body effective potential is (by definition)

$$V_2^{\text{exact}}(r) = \Phi(\mathcal{C}_r) - \Phi(\mathcal{C}_\infty). \quad (\text{B1})$$

Since $\Phi(\mathcal{C}_r)$ can be estimated from (A18), this quantity can be estimated. If one also considers the configuration $\mathcal{C}_{(0)}$ which has no large particles at all, and the configuration $\mathcal{C}_{(1)}$ with exactly one large particle, the exact one-body term in the CG model is

$$\Delta\mu^{\text{exact}} = \Phi(\mathcal{C}_{(0)}) - \Phi(\mathcal{C}_{(1)}), \quad (\text{B2})$$

which allows $\Delta\mu$ to be estimated by (A18). One may also fix $\Phi(\mathcal{C}_\infty) = 2\Phi(\mathcal{C}_{(1)}) - \Phi(\mathcal{C}_{(0)})$.

This procedure provides point estimates of V_2 at equally spaced values of r ; a smoothed estimate of V_2 is obtained by fitting to a continuous function, and then tabulated for use in simulations of the CG model. [See Fig. 6(a), discussed below in Appendix C]. A similar method enables computation of the three-body interaction potential V_3 , using systems with three large particles.

So far the method is identical to [27]. However, two aspects of the three-body potential are different from that work. First, we set $V_3(r_{12}, r_{23}, r_{13}) = 0$ unless $\sigma_B < r_{ij} < \sigma_B + 0.8\sigma_S$ for all pairs of particles. (It is expensive to estimate this function to high accuracy, so it is convenient to set it to zero in regions of space where its value is not much larger than the numerical error. Small errors in V_3 will be corrected by the two-level method in any case). We tabulate $V_3(x, y, z)$ for x, y, z on a cubic grid with spacing $\sigma_S/10$, and we use linear interpolation to estimate its value for generic arguments.

The second difference from [27] is that we compute V_3 based on a deterministically chosen set of large-particle

configurations (a random sample was used in [27]). These samples correspond to the points of the cubic grid described above, and the symmetry of V_3 under interchange of all arguments is ensured by ordering the arguments by increasing size.

We require high accuracy in these free-energy estimates so we use small values for the parameter δn that is used in the estimate of (A17). For V_2 we take $\delta n = 10^{-3}$ for $\eta_S^r \leq 0.2$, also $\delta n = 5 \times 10^{-4}$ for $0.2 < \eta_S^r \leq 0.3$, and $\delta n = 6.25 \times 10^{-5}$ for $0.3 < \eta_S^r \leq 0.35$. For computation of the three-body potential, larger systems are required (hence more expensive computations) but less accuracy is needed, so we increase δn by a factor of 2.5.

2. Computation of $\Delta\hat{p}$

In order to estimate Δp using (4), we take M representative configurations of the CG model, denoted by $\mathcal{C}_1, \dots, \mathcal{C}_M$, obtained by GCMC simulation of the CG model. For each sample, we compute $\hat{W}(\mathcal{C}_\alpha)$. Then define a normalized reweighting factor

$$\hat{\omega}_\alpha = \frac{\hat{W}(\mathcal{C}_\alpha)}{\frac{1}{M} \sum_{\beta=1}^M \hat{W}(\mathcal{C}_\beta)}. \quad (\text{B3})$$

With this choice, it is shown in [27] that (4) is an appropriate estimate of Δp , in the sense that its mean converges for large M to the true Δp , and its variance converges to zero [27]. We emphasize that this property holds even if the CG model is not accurate, although very large M may be required in that case.

We note that each estimate of $\hat{W}(\mathcal{C}_\alpha)$ requires a GCMC simulation for the small particles that may take several days on a single CPU core. However, all the \hat{W} computations are independent, allowing efficient use of high-performance (parallel) computing resources. In practice, we make four independent estimates of the weight \hat{W} for each coarse configuration; the average of these estimated weights is used as an unbiased estimate of the true weight.

For the results of the main text we take $M = 1280$. When computing the reweighting factors ω_α in the two-level method we take $\delta n = 10^{-2}$ for $\eta_S^r \leq 0.2$, also $\delta n = 5 \times 10^{-3}$ for $0.2 < \eta_S^r \leq 0.3$, and $\delta n = 6.25 \times 10^{-4}$ for $0.3 < \eta_S^r \leq 0.35$. (This is a suitable compromise between accuracy and computational time).

APPENDIX C: COARSE-GRAINED MODEL

1. Interaction potentials

Figure 6 illustrates the behavior of the effective interactions in the CG model. We give a brief description of its main properties.

Figure 6(a) shows the two-body effective interaction, which has the form of a depletion potential. There is a strong effective attraction between the particles, whose range is comparable with σ_S . Also, the layering of the small particles around the large ones means that the potential has oscillations, with both attractive and repulsive parts. We show results for parameters close to the critical point of the model, which are compared with the potential proposed by Roth, Evans, and Dietrich (RED) [21]. As previously noted in [33], the

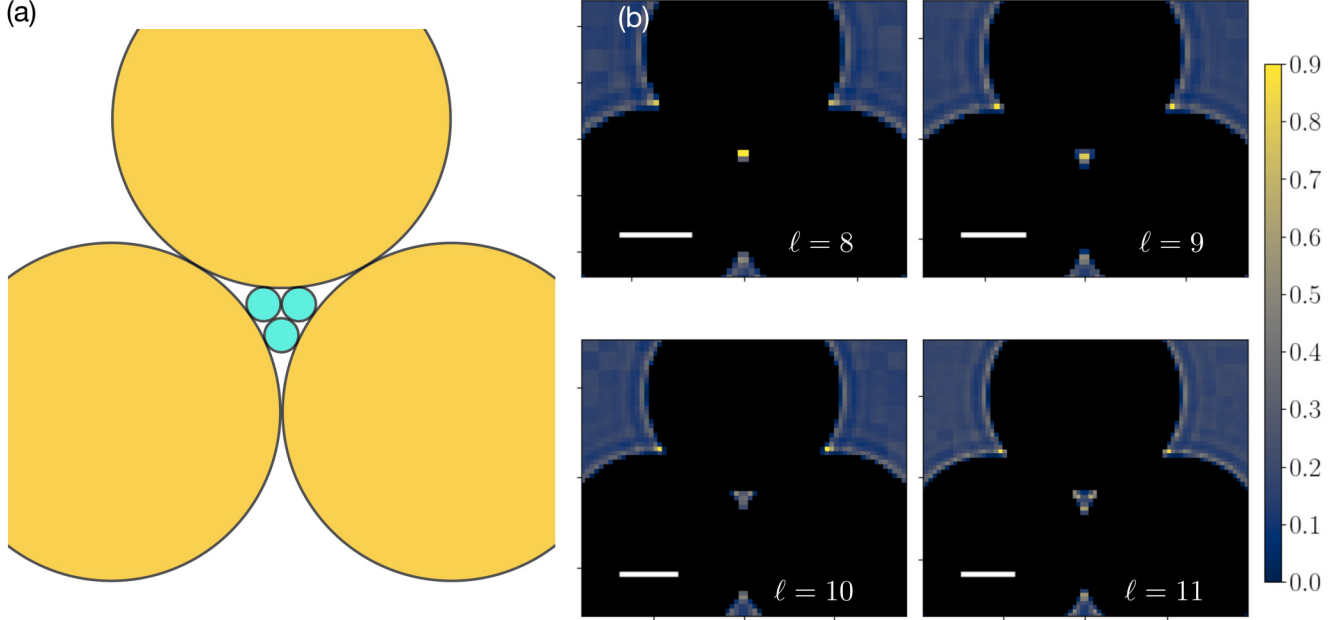


FIG. 7. (a) Illustration of the packing of small particles in the vicinity of three large ones. This (planar) configuration is possible for size ratios $\ell \geq 5 + \sqrt{24} = 9.90$. (b) Local density of small particles in the vicinity of three (fixed) large ones for $\eta_S^r = 0.32$ and $\ell = 8, 9, 10, 11$. In the case $\ell = 11$, three particles fit the gap, visible as three local peaks in the density. Scale bars are $3\sigma_s$.

RED potential is close to the true V_2 , but there are significant differences in the repulsive parts of these potentials. The error bars on V_2 are no larger than symbol sizes, hence the depletion potential is accurate.

Figure 6(b) shows how the strength of the depletion interaction depends on the size ratio ℓ and on η_S^r . This is quantified by the value of the depletion potential at contact. As expected, the potential gets stronger as ℓ and η_S^r increase.

By contrast, Fig. 6(c) indicates the strength of the three-body potential, for the specific case where all three particles are touching each other. (The strong two-body attraction means that this arrangement is the most common, so it is suitable for illustrative purposes). The three-body potential is smaller in absolute value than V_2 , and it may be either attractive ($V_3 < 0$) or repulsive ($V_3 > 0$). Note also that there is no clear trend for the dependence on η_S^r and ℓ : the potential may increase or decrease.

2. Three-body interactions

Figure 7 presents additional information to allow the behavior of V_3 to be rationalized. It shows the density of small particles in the vicinity of three large ones, which have fixed positions, all touching each other. For $\ell = 11$, three particles can fit into the (approximately) triangular region between the particles, while for $\ell \leq 10$, this does not occur. (Exactly at $\ell = 10$, three small particles can just fit in the planar arrangement of Fig. 7 but their positions are tightly constrained and the associated phase-space volume is extremely small. A similar effect can also be observed for packing of hard spheres in wedge-shaped geometries [76]). As a result, the packing for $\ell = 11$ is much more efficient than for $\ell = 10$, and the corresponding V_3 is smaller. By contrast, for $\ell = 8$, putting a single small particle into this region corresponds to a relatively

efficient packing and a smaller V_3 , at least compared with $\ell = 9, 10$.

These three-body effects have many subtle features. For the purposes of this work, two aspects are important. First, the potential at contact has values that are smaller than unity, but these are certainly not negligible contributions to the energy. Second, the sign of the interaction (and its dependence on η_S^r) has a nontrivial dependence on ℓ . Specifically, the three-body effect for $\ell = 10$ is significantly repulsive (and increasingly so at large η_S^r), while the corresponding effect for $\ell = 11$ is weakly repulsive for $\eta_S^r \approx 0.3$ but becomes attractive at larger η_S^r .

3. Accuracy of CG model

Recalling that a perfect coarse-grained model would have energy function $E_{CG}^{ex}(\mathcal{C}) = \Phi(\mathcal{C})$ (up to an additive constant), it is useful to define the Kullback-Leibler divergence between the Boltzmann distributions of our CG model and the exact one, which is

$$D_{KL}^{CG} = \sum_N \int d\mathbf{R}_1 \dots d\mathbf{R}_N p_{CG}(\mathcal{C}) \log[Z/W(\mathcal{C})] \quad (C1)$$

with $W(\mathcal{C})$ as in (A16). This D_{KL}^{CG} is non-negative and measures how different is the CG model from the exact one. It is zero if (and only if) the CG model is exact. This may be observed by writing it in the form

$$D_{KL}^{CG} = \langle E_{CG}^{ex}(\mathcal{C}) - E_{CG}(\mathcal{C}) \rangle_{CG} + \log \langle e^{E_{CG}(\mathcal{C}) - E_{CG}^{ex}(\mathcal{C})} \rangle_{CG}, \quad (C2)$$

which shows that it can be interpreted as the average coarse-graining error in E_{CG} .

In a free-energy perturbation theory computation [48], this quantity could be computed. In the method used here, the

$W(\mathcal{C})$ are not available but we do have their (unbiased) estimates $\hat{W}(\mathcal{C})$. Consider the quantity

$$\hat{D} = -\frac{1}{M} \sum_{\alpha} \log \hat{\omega}_{\alpha} \quad (\text{C3})$$

with $\hat{\omega}$ as in (B3), and recall that the configurations \mathcal{C}_{α} are representative samples from the CG model. Since $\hat{W}(\mathcal{C})$ is an unbiased estimate of $W(\mathcal{C})$, we have $\langle \hat{W}(\mathcal{C}_{\alpha}) \rangle_{\mathcal{J}} = W(\mathcal{C}_{\alpha})$ where $\langle \cdot \rangle_{\mathcal{J}}$ is the expectation value with respect to the stochastic computation of \hat{W} ; see also [27]. By (B3) we have

$$\langle \hat{D} \rangle_{\mathcal{J}} = -\frac{1}{M} \sum_{\alpha} \langle \log \hat{W}(\mathcal{C}_{\alpha}) \rangle_{\mathcal{J}} + \left\langle \log \frac{1}{M} \sum_{\alpha} \hat{W}(\mathcal{C}_{\alpha}) \right\rangle_{\mathcal{J}}. \quad (\text{C4})$$

For large M then $\frac{1}{M} \sum_{\alpha} \hat{W}(\mathcal{C}_{\alpha}) \approx \langle W \rangle_{\text{CG}} = Z$ (because the \mathcal{C}_{α} are representative CG configurations). Also, Jensen's

inequality means that $\langle \log \hat{W}(\mathcal{C}_{\alpha}) \rangle_{\mathcal{J}} \leq \log \langle \hat{W}(\mathcal{C}_{\alpha}) \rangle_{\mathcal{J}} = \log \hat{W}(\mathcal{C}_{\alpha})$. Using these facts we obtain

$$\langle \hat{D} \rangle_{\mathcal{J}} \gtrsim -\frac{1}{M} \sum_{\alpha} \log \hat{W}(\mathcal{C}_{\alpha}) + \log Z. \quad (\text{C5})$$

Finally using again that the \mathcal{C}_{α} are representative coarse configurations we have

$$\langle \hat{D} \rangle_{\mathcal{J}} \gtrsim \langle \log [Z / \hat{W}(\mathcal{C})] \rangle_{\text{CG}}. \quad (\text{C6})$$

The right-hand side is the KL divergence as in (C1), so we finally obtain

$$D_{\text{KL}}^{\text{CG}} \lesssim \langle \hat{D} \rangle_{\mathcal{J}} \quad (\text{C7})$$

That is, the computable quantity \hat{D} is an estimated upper bound for the error $D_{\text{KL}}^{\text{CG}}$ of the CG model.

-
- [1] J. P. Hansen and I. R. McDonald, *Theory of Simple Liquids*, 3rd ed. (Academic Press, London, 2005).
- [2] P. N. Pusey and W. van Meegen, *Nature (London)* **320**, 340 (1986).
- [3] S. Auer and D. Frenkel, *Nature (London)* **409**, 1020 (2001).
- [4] C. P. Royall, W. C. K. Poon, and E. R. Weeks, *Soft Matter* **9**, 17 (2013).
- [5] E. R. Weeks, J. C. Crocker, A. C. Levitt, A. Schofield, and D. A. Weitz, *Science* **287**, 627 (2000).
- [6] G. Parisi and F. Zamponi, *Rev. Mod. Phys.* **82**, 789 (2010).
- [7] J. de Graaf, R. van Roij, and M. Dijkstra, *Phys. Rev. Lett.* **107**, 155501 (2011).
- [8] G. van Anders, D. Klotsa, N. K. Ahmed, M. Engel, and S. C. Glotzer, *Proc. Natl. Acad. Sci. U. S. A.* **111**, E4812 (2014).
- [9] S. Sacanna, W. T. M. Irvine, P. M. Chaikin, and D. J. Pine, *Nature (London)* **464**, 575 (2010).
- [10] B. J. Alder and T. E. Wainwright, *J. Chem. Phys.* **27**, 1208 (1957).
- [11] W. W. Wood and J. D. Jacobson, *J. Chem. Phys.* **27**, 1207 (1957).
- [12] E. P. Bernard and W. Krauth, *Phys. Rev. Lett.* **107**, 155704 (2011).
- [13] P. F. Damasceno, M. Engel, and S. C. Glotzer, *Science* **337**, 453 (2012).
- [14] A. P. Gantapara, J. de Graaf, R. van Roij, and M. Dijkstra, *Phys. Rev. Lett.* **111**, 015501 (2013).
- [15] D. J. Ashton, R. L. Jack, and N. B. Wilding, *Phys. Rev. Lett.* **114**, 237801 (2015).
- [16] T. Biben and J.-P. Hansen, *Phys. Rev. Lett.* **66**, 2215 (1991).
- [17] Y. Rosenfeld, *Phys. Rev. Lett.* **72**, 3831 (1994).
- [18] Y. Rosenfeld, *J. Phys. Chem.* **99**, 2857 (1995).
- [19] M. Dijkstra, R. van Roij, and R. Evans, *Phys. Rev. Lett.* **81**, 2268 (1998).
- [20] M. Dijkstra, R. van Roij, and R. Evans, *Phys. Rev. E* **59**, 5744 (1999).
- [21] R. Roth, R. Evans, and S. Dietrich, *Phys. Rev. E* **62**, 5360 (2000).
- [22] W. C. K. Poon, *J. Phys.: Condens. Matter* **14**, R859 (2002).
- [23] S. Asakura and F. Oosawa, *J. Chem. Phys.* **22**, 1255 (1954).
- [24] H. N. W. Lekkerkerker, W. C.-K. Poon, P. N. Pusey, A. Stroobants, and P. B. Warren, *Europhys. Lett.* **20**, 559 (1992).
- [25] A. Buhot and W. Krauth, *Phys. Rev. Lett.* **80**, 3787 (1998).
- [26] M. Dijkstra, R. v. Roij, and R. Evans, *Phys. Rev. Lett.* **82**, 117 (1999).
- [27] H. Kobayashi, P. B. Rohrbach, R. Scheichl, N. B. Wilding, and R. L. Jack, *J. Chem. Phys.* **151**, 144108 (2019).
- [28] J. Largo and N. B. Wilding, *Phys. Rev. E* **73**, 036115 (2006).
- [29] A. Ayadim and S. Amokrane, *Phys. Rev. E* **74**, 021106 (2006).
- [30] M. López de Haro, C. F. Tejero, and A. Santos, *J. Chem. Phys.* **138**, 161104 (2013).
- [31] A. Santos, S. B. Yuste, and M. López de Haro, *J. Chem. Phys.* **153**, 120901 (2020).
- [32] D. Goulding and S. Melchionna, *Phys. Rev. E* **64**, 011403 (2001).
- [33] D. J. Ashton, N. B. Wilding, R. Roth, and R. Evans, *Phys. Rev. E* **84**, 061136 (2011).
- [34] M. Dijkstra, R. van Roij, R. Roth, and A. Fortini, *Phys. Rev. E* **73**, 041404 (2006).
- [35] J. Kolafa, S. Labik, and A. Malijevsky, *Phys. Chem. Chem. Phys.* **6**, 2335 (2004).
- [36] M. M. Tsypin and H. W. J. Blöte, *Phys. Rev. E* **62**, 73 (2000).
- [37] N. B. Wilding, *Phys. Rev. E* **52**, 602 (1995).
- [38] A. D. Bruce and N. B. Wilding, in *Advances in Chemical Physics*, edited by I. Prigogine and S. A. Rice (Wiley Online Library, 2003), Vol. 127, p. 1.
- [39] C. Jarzynski, *Phys. Rev. Lett.* **78**, 2690 (1997).
- [40] G. E. Crooks, *Phys. Rev. E* **61**, 2361 (2000).
- [41] R. M. Neal, *Stat. Comput.* **11**, 125 (2001).
- [42] G. Hummer and A. Szabo, *Proc. Natl. Acad. Sci. U. S. A.* **98**, 3658 (2001).
- [43] W. G. Noid, J.-W. Chu, G. S. Ayton, V. Krishna, S. Izvekov, G. A. Voth, A. Das, and H. C. Andersen, *J. Chem. Phys.* **128**, 244114 (2008).
- [44] M. Praprotnik, L. Delle Site, and K. Kremer, *J. Chem. Phys.* **126**, 134902 (2007).
- [45] T. E. Ouldridge, A. A. Louis, and J. P. K. Doye, *J. Chem. Phys.* **134**, 085101 (2011).
- [46] B. M. Mladek, J. Fornleitner, F. J. Martinez-Veracoechea, A. Dawid, and D. Frenkel, *Soft Matter* **9**, 7342 (2013).

- [47] A. J. Pak and G. A. Voth, *Curr. Opin. Struct. Biol.* **52**, 119 (2018).
- [48] R. W. Zwanzig, *J. Chem. Phys.* **22**, 1420 (1954).
- [49] B. Cheng, E. A. Engel, J. Behler, C. Dellago, and M. Ceriotti, *Proc. Natl. Acad. Sci. U. S. A.* **116**, 1110 (2019).
- [50] K. Binder and D. Heermann, *Monte Carlo Simulation in Statistical Physics* (Springer, Berlin, Heidelberg, 2019).
- [51] P. G. Debenedetti, F. Sciortino, and G. H. Zerze, *Science* **369**, 289 (2020).
- [52] M. G. Noro and D. Frenkel, *J. Chem. Phys.* **113**, 2941 (2000).
- [53] M. A. Miller and D. Frenkel, *Phys. Rev. Lett.* **90**, 135702 (2003).
- [54] H. Oberhofer and C. Dellago, *J. Comput. Chem.* **30**, 1726 (2009).
- [55] C. Vega, *J. Chem. Phys.* **108**, 3074 (1998).
- [56] G. Stell, *J. Stat. Phys.* **63**, 1203 (1991).
- [57] R. J. Baxter, *J. Chem. Phys.* **49**, 2770 (1968).
- [58] C. N. Likos, *Phys. Rep.* **348**, 267 (2001).
- [59] M. B. Giles, *Oper. Res.* **56**, 607 (2008).
- [60] D. F. Anderson and D. J. Higham, *SIAM Multiscale Modell. Simul.* **10**, 146 (2012).
- [61] V. H. Hoang, C. Schwab, and A. M. Stuart, *Inverse Probl.* **29**, 085010 (2013).
- [62] T. J. Dodwell, C. Ketelsen, R. Scheichl, and A. L. Teckentrup, *SIAM/ASA J. Uncertainty Quant.* **3**, 1075 (2015).
- [63] A. Beskos, A. Jasra, K. Law, R. Tempone, and Y. Zhou, *Stoch. Proc. Appl.* **127**, 1417 (2017).
- [64] T. J. Dodwell, C. Ketelsen, R. Scheichl, and A. L. Teckentrup, *SIAM Rev.* **61**, 509 (2019).
- [65] M. Rosin, L. Ricketson, A. Dimits, R. Caflisch, and B. Cohen, *J. Comput. Phys.* **274**, 140 (2014).
- [66] K. Jansen, E. H. Müller, and R. Scheichl, *Phys. Rev. D* **102**, 114512 (2020).
- [67] E. Løvbak, B. Mortier, G. Samaey, and S. Vandewalle, in *Computational Science—ICCS 2020*, edited by V. V. Krzhizhanovskaya, G. Závodszy, M. H. Lees, J. J. Dongarra, P. M. A. Sloot, S. Brissos, and J. Teixeira (Springer International, Cham, 2020), pp. 374–388.
- [68] A. Brandt and D. Ron, *J. Stat. Phys.* **102**, 231 (2001).
- [69] D. Ron, R. H. Swendsen, and A. Brandt, *Phys. Rev. Lett.* **89**, 275701 (2002).
- [70] A. Brandt and V. Ilyin, in *Multiscale Computational Methods in Chemistry and Physics*, edited by A. Brandt, J. Bernholc, and K. Binder (IOS Press, Amsterdam, 2001), pp. 187–197.
- [71] J. Behler and M. Parrinello, *Phys. Rev. Lett.* **98**, 146401 (2007).
- [72] A. P. Bartók, M. C. Payne, R. Kondor, and G. Csányi, *Phys. Rev. Lett.* **104**, 136403 (2010).
- [73] K. T. Schütt, H. E. Sauceda, P. J. Kindermans, A. Tkatchenko, and K. R. Müller, *J. Chem. Phys.* **148**, 241722 (2018).
- [74] T. E. Gartner, L. Zhang, P. M. Piaggi, R. Car, A. Z. Panagiotopoulos, and P. G. Debenedetti, *Proc. Natl. Acad. Sci. U. S. A.* **117**, 26040 (2020).
- [75] R. Roth, *J. Phys.: Condens. Matter* **22**, 063102 (2010).
- [76] M. Schoen and S. Dietrich, *Phys. Rev. E* **56**, 499 (1997).